Coherent quantum frequency bridge: phase preserving, nearly-noiseless parametric frequency converter

Ivan A. Burenkov[1,2,†], Y.-H. Cheng[1,2,†], Tim Thomay[1,2,†], Glenn S. Solomon[1,2], Alan L. Migdall[1,2], Thomas Gerrits[3,†], Adriana Lita[3], Sae Woo Nam[3], L. Krister Shalm[3,†], and Sergey V. Polyakov[2]

[1]Joint Quantum Institute & University of Maryland, College Park, MD 20742, USA
[2]National Institute of Standards and Technology, Gaithersburg, Maryland 20899, USA
[3]National Institute of Standards and Technology, Boulder, CO 80305, USA

ABSTRACT

We characterize an efficient and nearly-noiseless parametric frequency upconverter. The ultra-low noise regime is reached by the wide spectral separation between the input and pump frequencies and the low pump frequency relative to the input photons. The background of only ≈100 photons per hour is demonstrated. We demonstrate phase preservation in a frequency upconversion process at the single-photon level. We summarize our efforts to measure this ultra-low noise level, and discuss both single-photon avalanche photodiode measurements and a photon-counting transition edge sensor (TES) measurements. To reach the required accuracy, we supplemented our TES with a dark count reduction algorithm. The preservation of the coherence was demonstrated by simultaneously upconverting the input of each arm of a Mach-Zehnder interferometer through high interference fringe contrast. We observe fringe visibilities of ≥ 0.97 with faint coherent input.

Keywords: hybrid quantum system, ultra-low light measurements, single photon detector, parametric upconversion, statistical analysis

1. INTRODUCTION

Scalable processing of quantum information is one of the most important goals of modern quantum optics. Photons are often used to connect two or more quantum nodes. Coherent photon-matter interactions were demonstrated in various physical systems including atomic ensembles,[1] trapped ions,[2] quantum dots (QD),[3,4] and other systems. Each material system comes with a unique set of natural advantages and a narrow path to circumvent the natural disadvantages. In each case, scaling a quantum system up to meet the demands of a practical quantum circuit consisting of disparate components requires a major technological tour-de-force. In this regard, developing hybrid scalable quantum systems is an attractive path forward. The major obstacle for the practical use of hybrid systems, however, is that different material platforms favor photons of incompatible spectral characteristics. Coherent frequency conversion is an essential enabling tool for realizing scalable hybrid quantum systems.

For a faithful frequency conversion of a quantum state, both photon-number and phase information must be faithfully transferred to the output. Therefore, it is of critical importance to achieve sufficient coherence preservation and low background rates from the parametric process. An upconverter with a low background can in addition be used for a more efficient detection of telecom-band or (near)infrared quantum states.[5] Because the energy per photon in the telecom-band is considerably lower than in the visible, infrared detectors are often less efficient and suffer higher dark count rates (DCR)s than detectors of visible photons. Detection properties can be significantly improved in a hybrid detector.

A significant issue with parametric upconverters, however, is spontaneous generation of background photons in the output channel due to the strong optical pump. Much attention has been devoted to reducing this

[†]These authors contributed to this paper as guest researchers at National Institute of Standards and Technology
Further author information: (Send correspondence to I.A.B.)
I.A.B.: E-mail: ivan.burenkov@gmail.com, Telephone: 1 301 975 8112

background. The background is intrinsically suppressed by avoiding cascaded parametric processes[6] and by separating the signal and pump spectrally to minimize the overlap of the signal with the Raman spectrum. In addition, any spectrally-broad background can be partially reduced via elaborate passive filtering arrangements, with band pass filters (BPF)s as narrow as ≈0.01 nm full width at half maximum (FWHM).[7]

Our upconverter takes advantage of avoiding both cascaded parametric processes and Raman sidebands via a >600 nm spectral separation between the pump and input signal fields.[8,9] Measuring such a low rate of background events is a challenge. Using silicon single-photon avalanche diodes (SPAD)s with as few as <100 dark counts per second leads to statistically inconclusive results. We used an optical transition edge sensor (TES)[10] and introduced a dark count reduction algorithm for its readout. Our measurements show that our highly-efficient upconverter generates just ≈100 background photons per hour. The accuracy of our measurement compares favorably to that of the dimmest continuous sources of visible/NIR light ever reported (astrophysical objects of 30 AB magnitude or lower).[11] In this contribution, we present this measurement and all the previous attempts at characterizing this practically noiseless upconverter.

We also experimentally demonstrate that the coherence of a faint laser source is preserved upon upconversion. Therefore our experimental results are an enabling step towards the faithful upconversion of a large class of nonclassical photon states, including certain entangled states.

2. THE UPCONVERTER

The frequency upconverters studied here are two periodically poled, magnesium-oxide-doped periodically poled lithium niobate (MgO:PPLN) $\chi^{(2)}$ crystals with 10 mm long ridge waveguides. The crystals are quasi-phase matched (QPM) for the type-0 sum frequency generation (SFG) process of 919.5 nm and 1550 nm. In upconversion, background is typically generated by a strong pump beam that supplies photons at a signal wavelength and then upconverted to the output wavelength. This happens via either non-phasematched spontaneous downconversion of pump photons or Raman scattering. Notably, if the wavelength of a strong pump is longer than that of the signal, downconversion naturally cannot make photons at a signal wavelength. Then, large spectral detuning of the signal from the pump minimizes the effect of Raman scattering. Therefore, if a wavelength of 1550 nm is used as a pump and 919.5 nm is the signal input, we expect nearly background-free upconversion, and will refer to this configuration as "nearly background free" configuration. In this configuration the crystal is pumped with a continuous wave (CW) 1550 nm beam from a wavelength-stabilized diode laser, amplified with an optical fiber amplifier. We also study the conjugated process, with the strong pump at 919.5 nm and the signal at 1550 nm. For that, a home-built tunable external cavity diode laser in Littrow configuration at 919.5 nm is used as the pump. In the later case we expect background at least due to non-phasematched downconversion.

To characterize the conversion efficiency of our upconverters, we measure the upconverted power as a function of pump power. The measured coupling ratios of the lasers to the two PPLN waveguides, 28 %/37 % and 27 %/34 % for the wavelengths 919.5 nm/1550 nm respectively, are used to determine the internal quantum conversion efficiencies (defined as the number of upconverted photons divided by that of signal photons) of the PPLN waveguides (Fig. 1). The nearly linear trends, particularly at the maximum observed efficiency (above ≈50 %) show that, for the power range investigated in our setup, the efficiency of the QPM SFG process is limited only by the optical power of the pump.

3. DETECTORS

A conventional spectrometer with a cooled CCD matrix is used to characterize noise spectra of upconverter and phase matching with a single input optical beam.

To characterize background rates photon-counting equipment is used. Two conventional Si single-photon avalanche photodiodes (SPAD)s are used to make preliminary background noise characterization of the ultra-low noise upconverter and for the conjugated upconversion scheme. They are paired with a field-programmable gate array (FPGA) development board[12] to count detection events. Note that in our measurements dark counts (as low as just 5 counts per second for one of the SPADs!) turned out to be the limiting factors.

To circumvent this deficiency of our measurement, a custom-built TES (optimized for signal at 780 nm wavelength) is used for our high accuracy characterization of the background. The TES is maintained at a

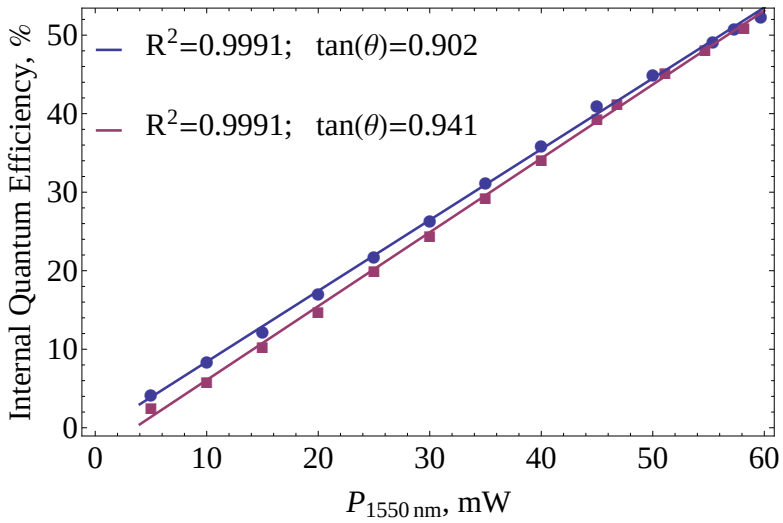

Figure 1. Measured internal quantum efficiencies of upconversion versus coupled pump power for two PPLN crystals. Solid lines: linear fits.

temperature below 0.1K with help of adiabatic demagnetization refrigerator. The temperature is monitored and data acquisition is suspended each time the temperature exceeds 0.1 K. The output of the TES is read by a superconducting quantum interference device (SQUID), amplified and processed by digitizing hardware. Each time the output voltage exceeds a chosen threshold, an associated waveform are recorded by a computer for further analysis. We study the dark count properties of the TES vs. threshold, and introduce other dark count reduction strategies based on processing of the raw TES output waveforms (See Experiment 2 section for details).

4. EXPERIMENT 1: COHERENCE PRESERVING UPCONVERSION

4.1 Experimental setup

To demonstrate preservation of phase in a parametric frequency mixing process, we set up a Mach-Zehnder interferometer with a frequency converter in each arm (Fig. 2), thereby making an interferometer with an output wavelength different from that of the two input wavelengths. For each channel in our setup the pump and the input beams are focused into the PPLN waveguide through an achromatic objective lens (numerical aperture ≈ 0.25). The waveguide temperature is maintained at ≈25 °C for the maximum conversion efficiency. The laser power of the 919.5 nm signal is attenuated to a range of 10^5 to 10^7 photons per second. Both the signal and pump beams are combined on a dichroic mirror (DM). Then, they are split into two channels with a polarizing beam splitter (PBS). The power splitting ratio is controlled with the half-wave plates before the DM. After splitting at the PBS, the beams are each upconverted to 577 nm. After wavelength conversion, the upconverted yellow light is collimated by an aspheric lens (numerical aperture ≈ 0.5). Then the 919.5 nm signal beam and residual background counts due to the strong pump are removed using a broad band-pass filter (BPF). The BPF is centered at 572 nm with a bandwidth of 28 nm, with a nominal 0.98 transmittance at 577 nm and a blocking optical density (OD) >7 at 919.5 nm. We use a mirror on a piezoelectric actuator to change the optical path difference between the two arms and observe interference fringes. To complete the interferometric measurement, we rotate the polarization of one beam so that the two beams have the same polarization when they are recombined on a non-polarizing beam-splitter (NPBS). An output port of the interferometer is coupled into a single-mode fiber (SMF) for detection. The SMF also acts as a spatial filter. We detect the upconverted faint state with a Si SPAD.

4.2 Results

Next we determine fringe visibility, defined as $\mathcal{V} = (R_{\max} - R_{\min})/(R_{\max} + R_{\min})$, where $R_{\max}$ and $R_{\min}$ are the maximum and minimum count rates, respectively at several input power levels. High-contrast fringes with visibilities of up to 0.98 are observed, shown in Fig. 3. To obtain $R_{\max}$ and $R_{\min}$, we fit their extrema with

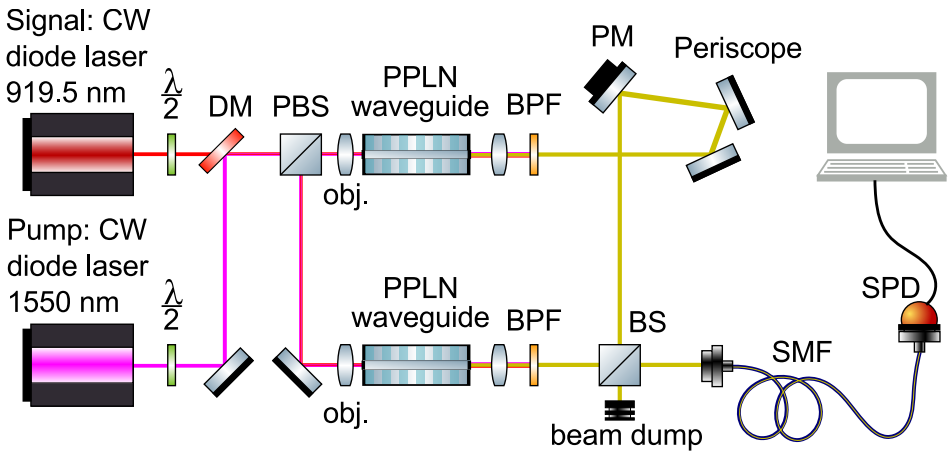

Figure 2. Phase preserving Mach-Zehnder interferometer upconversion setup. $\lambda/2$ - half-wave plate, NDF - neutral-density filter, DM - dichroic mirror, PBS - polarizing beam-splitter, obj. - objective lens, asphere - aspheric collimation lens, BPF - band-pass filter, PM - mirror on a piezoelectric actuator, NPBS - non-polarizing beam-splitter, SMF - single-mode fiber, SPD - single-photon detector, see text.

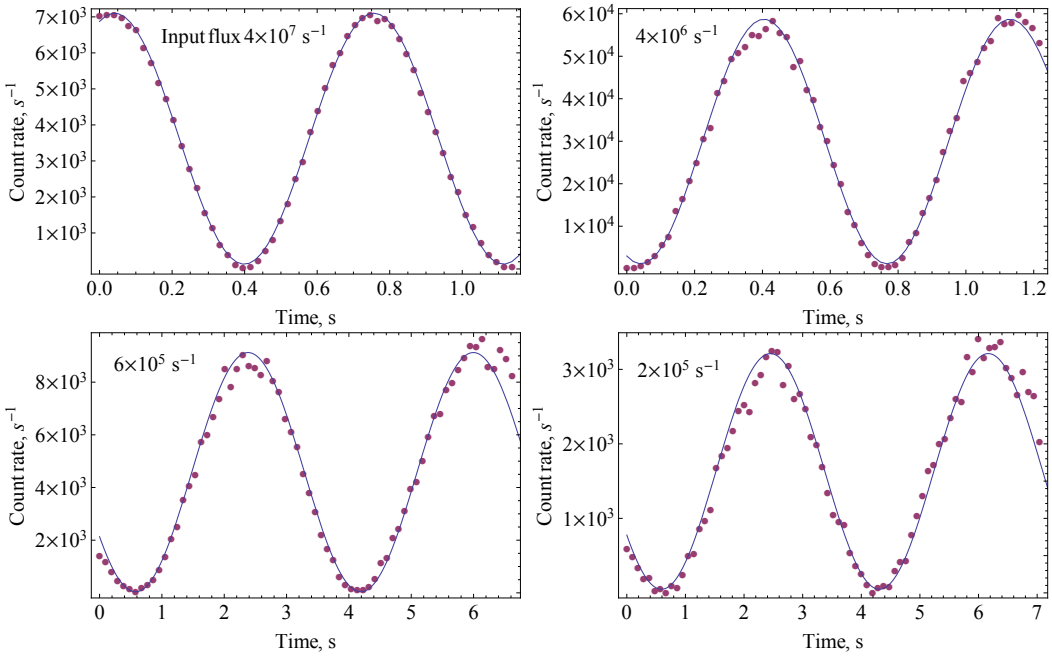

Figure 3. Experimental demonstration of the interference fringes (dots: data; line: sine fit, provided as a guide to the eye) between the two upconverted beams with faint coherent state input at 919.5 nm at four input light levels.

parabolas, and averaged over at least 16 extrema. We use this method rather than fitting sine functions to reduce the effect of the nonlinear behavior of the piezoelectric actuator.

The raw visibility is summarized in Table 1. Notice it drops for lower fluxes. To better understand this, we subtract the independently measured detector DCR from fringes. We see that correcting solely for the detector DCR restores high visibility at lower input fluxes. Thus, the observed visibility loss is solely due to the detector performance, and not a property of an upconverting interferometer.

Table 1. Observed visibilities for four different 919.5 nm photon fluxes.

methods \ input light flux (s^{-1})	$4{\cdot}10^7$	$4{\cdot}10^6$	$6{\cdot}10^5$	$2{\cdot}10^5$
extrema with local fits	0.98(1)	0.98(1)	0.96(2)	0.93(1)
extrema with local fits and subtraction of DCR	0.98(1)	0.98(1)	0.98(2)	0.97(1)

5. EXPERIMENT 2: BACKGROUND MEASUREMENTS

5.1 Experimental setup

In the experiment (Fig. 4), both the signal and pump beams are combined on a dichroic mirror (DM) before the upconverting crystal. Both lasers are used simultaneously only for alignment and to characterize the quantum efficiency of the upconversion setup (see above). To measure the background of the upconverter, only the pump laser is used, while the input signal laser is blocked. Experimental setups are identical for both crystals. Preliminary noise measurements are performed with two SPADs with low dark count rates. In both cases the upconverters are statistically background-free, because of the SPAD's dark count properties. The initial measurement with a Si SPAD detector with ≈85 dark counts per second gives the uncertainty of 2 photons/s. In the subsequent measurement we improve the internal conversion efficiency by more than a factor of 2 and replace the original SPAD with an extremely low dark count SPAD (with ≈5 dark counts per second). Even with this arrangement we are unable to measure statistically significant background noise from the upconverter (see Table 2). To reach the accuracy required for this measurement, we employed an optical transition edge sensor (TES) and optimized its dark count rate.

Unlike Si-based SPADs, the TES can detect photons at 1550 nm, our pump wavelength. We added an extra low-pass filter with an additional OD >7 at 1550 nm to ensure that pump photons are not impinging on a TES. The attenuation of the residual pump from the other optical components adds up to more than 5 additional orders of magnitude. The output is then coupled to a single-mode fiber for further analysis. Note that the only requirement for a filter in this upconverter is to block pump wavelengths (1550 nm or 919.5 nm, depending on a configuration) and their second harmonics (775 nm or 460 nm, respectively).[8] We characterize the background with two different PPLN crystals to show that the low-background feature of this upconversion process is repeatable.

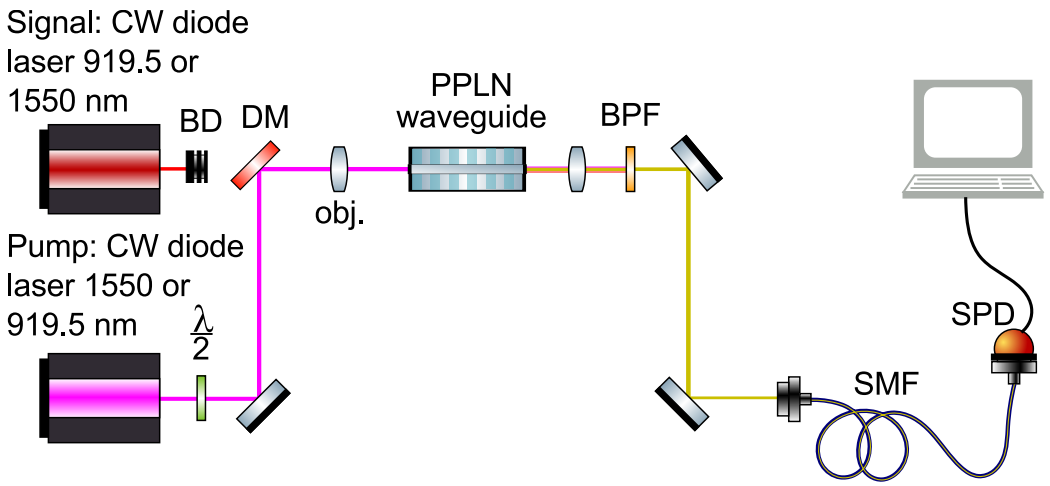

Figure 4. Noise characterization upconversion setup.

5.2 TES calibration and dark count reduction

Photons of different wavelengths differ in energy and result in TES output waveforms of different amplitudes and FWHM.[13,14] For photons of a particular wavelength, a spread of waveforms is generated. The first step in calibrating a TES is to determine a variation in waveform parameters with photon wavelength. This information

is used to select a proper threshold. In Fig. 6, the raw DCR is presented vs. the amplitude discrimination threshold. To obtain this dependence we tightly cap the optical fiber input port and record calibrating waveforms. Then we calculate the number of waveforms with peak amplitudes higher than a certain voltage level. The raw DCR data is shown along with the TES response to 577 nm photons, see Fig. 6. To obtain the signal TES response, we attenuate the upconverted light to $\approx 10^4$ photons per second and collect 10^4 TES waveforms. Using these measurements we select a trigger value of $V_0 = 20$ mV for the main data acquisition. This threshold allows for flexibility in post-processing while limiting the number of stored waveforms by excluding most of dark count events. This raw DCR data also helps us estimate what the DCR of the same detector would be with a longer-wavelength input. Note that this threshold results in a modest reduction of the detection efficiency of about 4 %, due to the high value of V_0, but significantly reduces DCR.

Next, we take advantage of the TES detection waveform properties to implement a DCR reduction. To use both amplitude and duration as the selection criteria in post-processing, we build a 2D histogram of amplitudes and FWHM durations of the waveforms due to 577 nm photons (Fig. 5(a)). Using this diagram we have defined waveform bounds for the upconverted photons that are subsequently applied to dark and background rate measurements. This processing reduces the number of the above-threshold events by excluding odd-looking waveforms that cannot be attributed to detection of photons at the wavelength of interest.

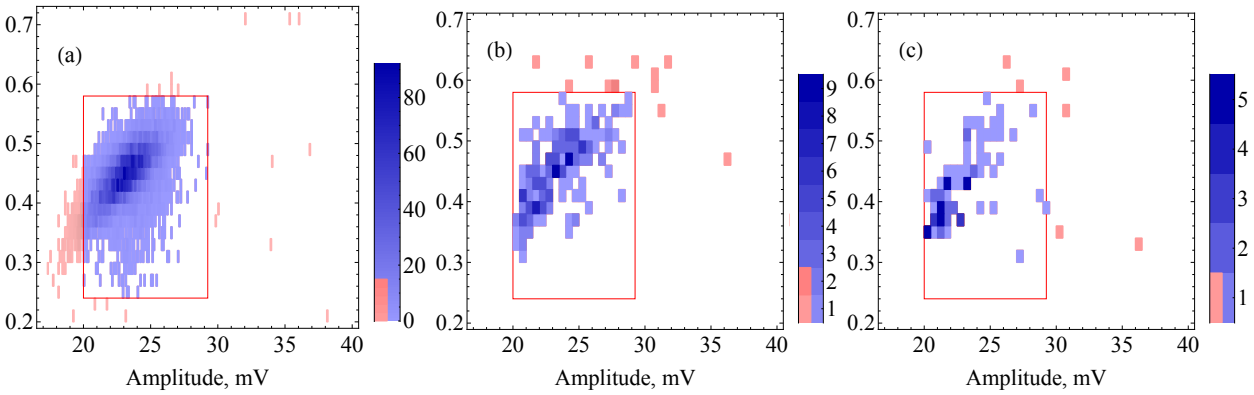

Figure 5. TES waveform histograms of amplitudes versus FWHM durations for (a) attenuated upconverted light $t_{\text{exposure}} \approx 1$ s, $N_{\text{waveforms}} = 10000$, (b) upconversion background noise $t_{\text{exposure}} = 4 \times 10^4$ s, number of accepted waveforms $N_{\text{waveforms}} = 203$, (c) DCR $t_{\text{exposure}} = 4 \times 10^4$ s, number of accepted waveforms $N_{\text{waveforms}} = 91$. Red rectangle shows the bounds on duration and amplitude used in waveform post-selection. Gradient of blue color used to show accepted waveforms, red gradient represents rejected waveforms. Note: not all rejected waveforms are shown, because their amplitudes and/or durations exceed the axes limits in this plot.

In characterizing the DCR, we obtained 0.0033(3) raw events per second. After applying constraining thresholds, the DCR is reduced to 0.0023(2) detections per second. Owing to such a low DCR, we make measurements with a record absolute accuracy. A test of temporal variations of the DCR was made by interspersing background measurements with DCR measurements. No statistically significant deviations of the DCR were seen.

The TES used for our measurements is optimized to have nearly 100 % efficiency at 780 nm and required a separate calibration for 577 nm. We calibrated it against a tarp detector[15] using light generated by the upconverter. The trap detector had a detection efficiency of ≈99.5 % with a spatial nonuniformity of <0.1 %. We used a detector substitution calibration method with the aid of a set of pre-calibrated attenuators. Before measuring detection efficiency, discrimination thresholds on the TES output were set as described above. Our measurement yielded a detection efficiency of 60(5) % at the target wavelength on constrained TES waveforms.

5.3 Results

In a first preliminary measurement we use ≈70 mW of 1550 nm pump - the maximal available power from the laser. We accurately evaluate the dark count rate of the Si detector, then measure background of the upconverters. To verify against any deviations from the expected statistical properties of the photoelectronic detections, these

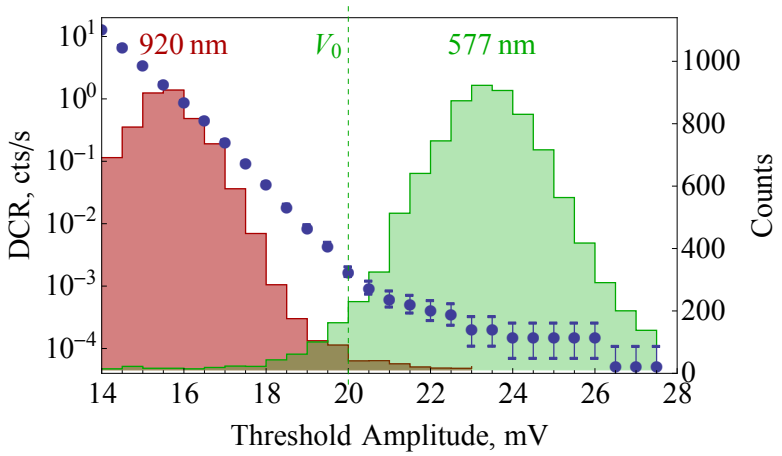

Figure 6. Distribution of detected TES waveforms vs. discriminating amplitude threshold level. An integrated amplitude histogram of counts above threshold value with no input light (blue dots, error bars correspond to standard deviation of measured counts, logarithmic scale); measured peak amplitude histograms of 10000 detection events for 577 nm (green) and 920 nm (red), labeled and shown on a linear scale (right vertical scale). The choice of the threshold V_0 defines the TES wavelength sensitivity and DCR.

measurements are interspersed. We find, to the statistical accuracy of this measurement, that the statistical behavior of the output supports the expected underlying stationary Poisson distribution of the recorded events. Therefore, the statistical uncertainty follows the shot noise limit. To find the true optical background photon flux due to upconversion, we subtract the measured dark count rate from the measured background count rate, factor in the measured optical losses and propagate the uncertainties. We find that the generated background photon flux is indistinguishable from zero to within the uncertainty for this SPAD (SPAD 1, see Table 2).

In a second preliminary measurement, we supplement the 1550 laser source with an optical amplifier and used ≈150 mW as a pump - the maximal recommended input power for our crystal. We used the low-noise SPAD 2 with a dark count rate of just 5 counts per second. Again, we find that the generated background photon flux is indistinguishable from zero to within the uncertainty.

For the high-accuracy accurate background measurements we replaced the SPAD with a TES. Again, we take interspersed measurements: each measurement of a background is followed by a DCR measurement. The exposure time of each measurement is 10^4 s. This measurement sequence was repeated four times. Full raw datasets obtained in a background measurement and a DCR measurement for the first waveguide are shown in Fig. 7(a) and Fig. 7(b) correspondingly. In the next step, we produce 2D histograms of the waveforms and apply pre-determined constraints to the background (Fig. 5(b)) and a DCR (5(c)) measurements. All collected waveforms are color-coded as accepted (blue) and rejected (red) in Fig. 7. At the TES detector, we measured the background to be just 0.0028(4) photons per second after subtracting the DCR. Then, we calculated the generated background by factoring in optical losses upstream. This method yields a background noise rate of 0.028(4) photons per second for waveguide 1 (See Table 1) for estimated efficiency of 10(1) %. Our measurement on the second waveguide resulted in a comparable value for the background noise, albeit with slightly higher absolute uncertainty (See Table 1).

We also characterize the conjugated process: i.e. with a pump laser at 919.5 nm and signal at 1550 nm. Here we use ≈80 mW of 919.5 nm pump - the maximum available power. Unlike for the inherently noiseless configuration, we observe a significant level of background counts. Therefore, this background is measured with a low-DCR silicon SPAD. Notice that the background in this configuration is nearly 10^6 higher than that in an inherently noiseless configuration (see Table 1). This result confirms a clear advantage of long-wavelength-pumped upconversion (c.f.[6]), i.e. shows significance of spontaneous non-phasematched processes detuned from the strong pump by as much as 600 nm!

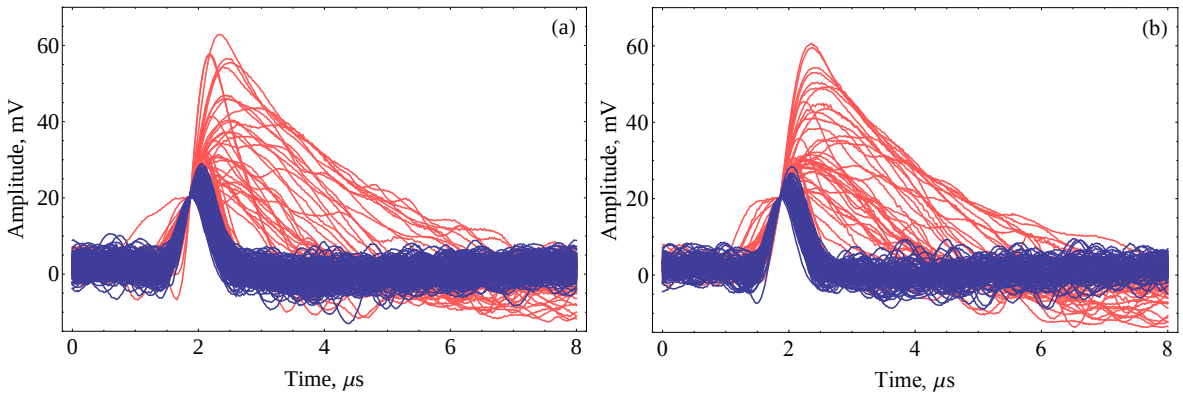

Figure 7. Measurement of the upconverter's background. TES waveforms collected in a 4×10^4 s measurements (a) for background upconversion noise; (b) dark counts. Waveforms that are inside the bounds given in Fig 5 are shown in blue, and the others are shown in red.

Table 2. Performance of the upconverters measured by two detectors (TES and SPAD) at the output wavelength of 577 nm. Two pump wavelengths λ_{pump}, 1550 nm and 920 nm, were tested. The efficiency of the SFG process is defined as the upconverted photons/incident photons. The DCR for the SPAD is the due to the detector alone. The DCR for the TES includes some amount of light leakage into the long fiber needed to reach the location of the TES system. The SFG background as measured is the photon count rate minus the DCR. This value includes losses due to optics transmission, coupling, and detection inefficiency. The inferred value is that same rate adjusted for those losses to obtain the background generated by the SFG process alone. One standard deviation statistical uncertainties are indicated.

Configuration	λ_{pump}, nm	SFG efficiency	DCR, cts/s	SFG background, cts/s	
				(as measured)	(inferred)
PPLN #1 SPAD 1	1550	20 %	84.0(3)	-0.1(4)	-1(2)
PPLN #1 SPAD 2	1550	53 %	5.23(5)	0.00(6)	0.00(15)
PPLN #1 TES	1550	53 %	0.0023(2)	0.0028(4)	0.028(4)
PPLN #2 TES	1550	41 %	0.0024(5)	0.0033(9)	0.039(10)
PPLN #1 SPAD 2	920	13 %	5.2(5)	7500(100)	17000(200)

6. EXPERIMENT 3: PHASE-MATCHING CHARACTERIZATION WITH A SINGLE OPTICAL INPUT

While high background in short-wavelength-pumped configuration is a clear deficiency for upconversion at a single photon level, the spectral properties of this upconverted background can be used for taking phase matching curves of a nonlinear crystal with just one input beam. To do so, one can send a short wavelength pump to the crystal and observe the spectra of noise using a low-noise spectrometer. Then, either a pump wavelength is scanned or the temperature of the crystal is changed, and the output spectrum is measured. Finally, the energy conservation relation is used to infer the matching long-wavelength signal. Here, we measured a temperature tuning curve for a constant pump wavelength. In Fig. 8 we show measurements at three different crystal temperatures: i.e. a part of a temperature tuning curve. With the aid of this measurement, it is easy to adjust pump and signal lasers and fine-tune the temperature to ensure the best performance of an upconverter. Because the background photon flux is high enough to be detectable by conventional optical spectrometers, one can easily obtain these phase matching curves with the help of a short-wavelength laser only, i.e. without the time consuming two-beam alignment.

7. DISCUSSION AND CONCLUSIONS

We summarize our efforts in characterizing a nearly-noiseless highly efficient upconverting frequency bridge. The background generated by the upconverter in its inherently noiseless configuration is 0.028(4) photons per second. We saw conversion efficiency as high as 53 % with no signs of saturation; theoretically, conversion efficiency could

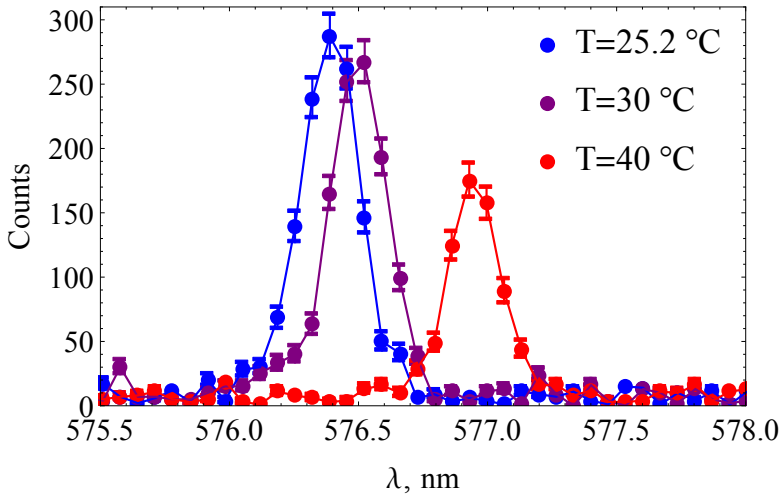

Figure 8. Upconverter output spectra due to random phase matching of short-wavelength pump and pump induced wideband background noise for different temperatures of PPLN crystal. Error bars correspond to standard deviation of measured counts.

reach 100 %.[16] To our knowledge, these noise measurements demonstrate a new level in faint light source photon flux measurement, providing better accuracy in 100 times shorter measurement (as compared to Hubble Space Telescope extremely deep field data,[11]). Because a parametric process is phase-preserving,[8,17–19] it can be used to faithfully convert a broad range of non-classical states including entangled states.

We point out that this upconverter can be used to enhance the range of efficient noiseless detection. Because the energy of the output photons is significantly higher than that of the input photons, one can use single-photon detectors with a higher discrimination threshold. In this upconverter, the output wavelength matches the peak efficiency of silicon-based detectors. We evaluated the effect of using upconverted photons vs. 920 nm photons with this TES. A histogram of pulse amplitudes due to the 920 nm photons along with the measured DCR at that amplitude levels shows that the TES DCR is elevated at least 4 fold for 920 nm vs 577 nm detection (Fig. 6). Therefore, to improve signal-to noise ratio, detecting photons upconverted in this low-noise upconverter is more advantageous than a direct detection of 920 nm photons in a TES. We expect that the relative reduction in the DCR by employing a similar upconverter vs. a direct TES detection will be even more significant for input light at longer wavelengths. We have therefore demonstrated the possibility of extending ultra-low-darkcount photon detection to the infrared via our nearly-noiseless upconversion.

Further, we have experimentally shown that quantum frequency upconversion maps, with high fidelity, the phase information of an input signal onto the upconverted light at the single-photon compatible level (we demonstrated fringe visibility of ≈0.98). Together with high fidelity upconversion of single-photon states, reported elsewhere,[17] this result will be particularly useful for upconverting certain entangled states.[20] The current experimental setup is nearly identical to what would be required for this. Converting our setup for the upconversion of entangled states requires removing the periscope and replacing the last NPBS before the detection by a PBS to properly recombine the two polarization components of the upconverted state.

REFERENCES

[1] Julsgaard, B., Sherson, J., Cirac, J. I., Fiurasek, J., and Polzik, E. S., "Experimental demonstration of quantum memory for light," *Nature* **432**, 482–486 (Nov. 2004).

[2] Blatt, R. and Wineland, D., "Entangled states of trapped atomic ions," *Nature* **453**, 1008–1015 (June 2008).

[3] De Greve, K., Yu, L., McMahon, P. L., Pelc, J. S., Natarajan, C. M., Kim, N. Y., Abe, E., Maier, S., Schneider, C., Kamp, M., Hofling, S., Hadfield, R. H., Forchel, A., Fejer, M. M., and Yamamoto, Y., "Quantum-dot spin-photon entanglement via frequency downconversion to telecom wavelength," *Nature* **491**, 421–425 (Nov. 2012).

[4] Gao, W. B., Fallahi, P., Togan, E., Miguel-Sanchez, J., and Imamoglu, A., "Observation of entanglement between a quantum dot spin and a single photon," *Nature* **491**, 426–430 (Nov. 2012).

[5] Vandevender, A. P. and Kwiat, P. G., "High efficiency single photon detection via frequency up-conversion," *Journal of Modern Optics* **51**(9-10), 1433–1445 (2004).

[6] Pelc, J. S., Ma, L., Phillips, C. R., Zhang, Q., Langrock, C., Slattery, O., Tang, X., and Fejer, M. M., "Long-wavelength-pumped upconversion single-photon detector at 1550 nm: performance and noise analysis," *Opt. Express* **19**, 21445 (Oct 2011).

[7] Kuo, P. S., Pelc, J. S., Slattery, O., Kim, Y.-S., Fejer, M. M., and Tang, X., "Reducing noise in single-photon-level frequency conversion," *Opt. Lett.* **38**, 1310 (2013).

[8] Cheng, Y.-H., Thomay, T., Solomon, G. S., Migdall, A. L., and Polyakov, S. V., "Statistically background-free, phase-preserving parametric up-conversion with faint light," *Opt. Express* **23**, 18671–18678 (Jul 2015).

[9] Burenkov, I. A., Gerrits, T., Lita, A., Nam, S. W., Shalm, L. K., and Polyakov, S. V., "Quantum frequency bridge: high-accuracy characterization of a nearly-noiseless parametric frequency converter," *Opt. Express* **25**, 907–917 (Jan 2017).

[10] Lita, A. E., Miller, A. J., and Nam, S. W., "Counting near-infrared single-photons with 95% efficiency," *Opt. Express* **16**, 3032–3040 (Mar 2008).

[11] Illingworth, G. D., Magee, D., Oesch, P. A., Bouwens, R. J., Labb, I., Stiavelli, M., van Dokkum, P. G., Franx, M., Trenti, M., Carollo, C. M., and Gonzalez, V., "The hst extreme deep field (xdf): Combining all acs and wfc3/ir data on the hudf region into the deepest field ever," *The Astrophysical Journal Supplement Series* **209**(1), 6 (2013).

[12] *physics.nist.gov/fpga*.

[13] Pearlman, A. J., Polyakov, S. V., Migdall, A., and Nam, S. W., "Number-resolving, single photon detection with no deadtime," in [*Conference on Lasers and Electro-Optics/Quantum Electronics and Laser Science Conference and Photonic Applications Systems Technologies*], *Conference on Lasers and Electro-Optics/Quantum Electronics and Laser Science Conference and Photonic Applications Systems Technologies* , JThA56, Optical Society of America (2008).

[14] Polyakov, S. V., Migdall, A., and Nam, S. W., "Real-time data-acquisition platform for pulsed measurements," *AIP Conference Proceedings-American Institute of Physics* **1327**, 505–519 (2011).

[15] Fox, N. P., "Trap detectors and their properties," *Metrologia* **28**(3), 197 (1991).

[16] Boyd, R. W., [*Nonlinear Optics, Third Edition*], Academic Press, 3rd ed. (2008).

[17] Ates, S., Agha, I., Gulinatti, A., Rech, I., Rakher, M. T., Badolato, A., and Srinivasan, K., "Two-photon interference using background-free quantum frequency conversion of single photons emitted by an InAs quantum dot," *Phys. Rev. Lett.* **109**, 147405 (Oct 2012).

[18] Ceus, D., Delage, L., Grossard, L., Reynaud, F., Herrmann, H., and Sohler, W., "Contrast and phase closure acquisitions in photon counting regime using a frequency upconversion interferometer for high angular resolution imaging," *Monthly Notices of the Royal Astronomical Society* **430**(3), 1529–1537 (2013).

[19] Gomes, J.-T., Delage, L., Baudoin, R., Grossard, L., Bouyeron, L., Ceus, D., Reynaud, F., Herrmann, H., and Sohler, W., "Laboratory demonstration of spatial-coherence analysis of a blackbody through an up-conversion interferometer," *Phys. Rev. Lett.* **112**, 143904 (Apr 2014).

[20] Flagg, E. B., Polyakov, S. V., Thomay, T., and Solomon, G., "A quantum eraser-based entangled photon source," *to be submitted* .